LETTERS

A hemispherical electronic eye camera based on compressible silicon optoelectronics

Heung Cho Ko[1]*, Mark P. Stoykovich[1]*, Jizhou Song[2], Viktor Malyarchuk[3], Won Mook Choi[1], Chang-Jae Yu[1], Joseph B. Geddes III[4], Jianliang Xiao[7], Shuodao Wang[7], Yonggang Huang[7,8] & John A. Rogers[1,2,3,4,5,6]

The human eye is a remarkable imaging device, with many attractive design features[1,2]. Prominent among these is a hemispherical detector geometry, similar to that found in many other biological systems, that enables a wide field of view and low aberrations with simple, few-component imaging optics[3–5]. This type of configuration is extremely difficult to achieve using established optoelectronics technologies, owing to the intrinsically planar nature of the patterning, deposition, etching, materials growth and doping methods that exist for fabricating such systems. Here we report strategies that avoid these limitations, and implement them to yield high-performance, hemispherical electronic eye cameras based on single-crystalline silicon. The approach uses wafer-scale optoelectronics formed in unusual, two-dimensionally compressible configurations and elastomeric transfer elements capable of transforming the planar layouts in which the systems are initially fabricated into hemispherical geometries for their final implementation. In a general sense, these methods, taken together with our theoretical analyses of their associated mechanics, provide practical routes for integrating well-developed planar device technologies onto the surfaces of complex curvilinear objects, suitable for diverse applications that cannot be addressed by conventional means.

The ability to implement electronic and optoelectronic systems on non-planar surfaces could be useful not only for hemispherical cameras and other classes of bio-inspired device designs, but also for conformal integration on or in biological systems as monitoring devices, prosthetics and so on. Unfortunately, existing technologies have been developed only for surfaces of rigid, semiconductor wafers or glass plates and, in more recent work, flat plastic sheets and slabs of rubber. None is suitable for the application contemplated here because the mechanical strains needed to accomplish the planar to hemispherical geometrical transformation (for example up to ~40% for compact eye-type cameras) greatly exceed the fracture strains (for example a few percent) of all known electronic materials, particularly the most well-developed inorganics, even in 'wavy' structural layouts[6].

One strategy to circumvent these limitations involves adapting all of semiconductor processing and lithography for direct use on curvilinear surfaces. Even a single part of this type of multifaceted procedure—for example lithographic patterning on such surfaces[7–15] (see also the Ball Semiconductor website, http://www.ballsemi.com/) with levels of resolution and multilevel registration that begin to approach those that can be easily achieved on planar surfaces—requires solutions to extremely difficult technical challenges. Although some work based on plastic deformation of planar sheets[16,17], self-assembly of small chips[18,19] and folding of elastic membranes[20,21] have shown some promise, each has drawbacks and all require certain processing steps to

be performed on a hemispherical or curved surface. Partly as a result, none have been used to achieve the type of cameras contemplated here.

In this paper, we introduce a means of producing curvilinear optoelectronics and electronic eye imagers that uses well-established electronic materials and planar processing approaches to create optoelectronic systems on flat, two dimensional surfaces in unusual designs that tolerate compression and stretching to large levels of strain (~50% or more). Conceptually this feature enables planar layouts to be geometrically transformed (that is conformally wrapped) to nearly arbitrary curvilinear shapes. In the example presented here, we use a hemispherical, elastomeric transfer element to accomplish this transformation with an electrically interconnected array of single-crystalline silicon photodiodes and current-blocking p–n junction diodes assembled in a passive matrix layout. The resulting hemispherical focal plane arrays, when combined with imaging optics and hemispherical housings, yield electronic cameras that have overall sizes and shapes comparable to the human eye. Experimental demonstrations and theoretical analyses reveal the key aspects of the optics and mechanics of these systems.

Figure 1 illustrates the main steps in the fabrication. The process begins with the formation of a hemispherical, elastomeric transfer element by casting and curing a liquid prepolymer to poly(dimethyl-siloxane) (PDMS) in the gap between opposing convex and concave lenses with matching radii of curvature (~1 cm). A jig specially designed to hold these lenses also provides a raised rim around the perimeter of the resulting piece of PDMS. This transfer element is mounted into a mechanical fixture that provides coordinated radial motion of ten independent paddle arms that each inserts into the rim. Translating the arms of this radial tensioning stage outwards expands the hemisphere. The associated reversible, elastic deformations in the PDMS transform this hemisphere, at sufficiently large tension, into the planar shape of a 'drumhead', such that all points in the PDMS are in biaxial tension. The extent of expansion and the underlying mechanics determine the overall magnitude of this tension.

Separately, conventional planar processing forms a passive matrix focal plane array on a silicon-on-insulator wafer consisting of single-crystalline silicon photodetectors, current-blocking p–n junction diodes and metal (chromium–gold–chromium) interconnects, with films of polymer (polyimide) to support certain regions and to encapsulate the entire system. A critically important design feature is the use of thin, narrow lines to connect nearest-neighbour pixel elements; these structures enable elastic compressibility in the system, as described below. Removing the buried oxide layer of the silicon-on-insulator wafer by etching with concentrated hydrofluoric acid in a manner that leaves the focal plane array supported by polymer posts

[1]Department of Materials Science and Engineering, [2]Department of Mechanical Science and Engineering, [3]Frederick-Seitz Materials Research Laboratory, [4]Beckman Institute for Advanced Science and Technology, [5]Department of Electrical and Computer Engineering, [6]Department of Chemistry, University of Illinois at Urbana-Champaign, Urbana, Illinois 61801, USA. [7]Department of Mechanical Engineering, [8]Department of Civil and Environmental Engineering, Northwestern University, Evanston, Illinois 60208, USA.
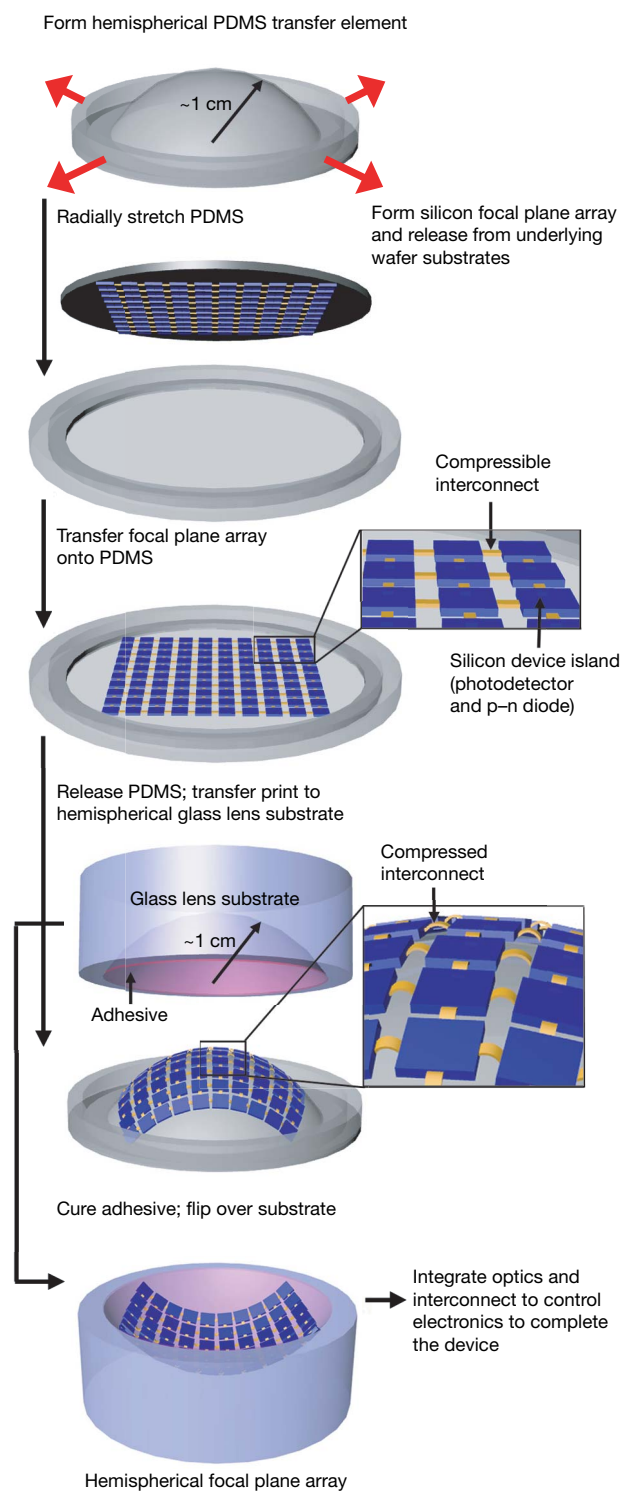*These authors contributed equally to this work.

Figure 1 | Illustration of steps for using compressible silicon focal plane arrays and hemispherical, elastomeric transfer elements to fabricate electronic eye cameras. The top frame shows such a transfer element, fabricated in PDMS by casting and curing against an appropriately designed template. Stretching in the radial direction forms a flat drumhead membrane in which all points in the PDMS are in tension. Lifting a prefabricated focal plane array and associated electronics from a source wafer onto the surface of this drumhead, and then allowing the PDMS to relax back to its initial shape, transforms the planar device layout into a hemispherical shape. Transfer printing onto a matching hemispherical glass substrate coated with a thin layer of a photocurable adhesive (pink), adding a hemispherical cap with integrated imaging lens and interfacing to external control electronics (not shown here) completes the camera system.

but otherwise raised above the underlying silicon 'handle' wafer completes the device processing. Fabrication of the interconnected pixel arrays on rigid, planar substrates using established processing techniques avoids limitations, for example in registration, that are often encountered in soft electronics. (Fabrication details appear in the Supplementary Information.)

Bringing the transfer element in its tensioned, planar drumhead shape into contact with this wafer and then peeling it away lifts up the focal plane array, leaving it stuck to the soft surface of the elastomer through non-specific van der Waals interactions[22,23]. Moving the paddle arms of the tensioning stage inwards to their initial positions causes the elastomer to relax back, approximately, to its initial hemispherical shape but with a slightly (~10% for the systems investigated here) larger radius of curvature. In this process, compressive forces act on the focal plane array to bring the pixel elements closer together, with magnitudes that correspond to significant compressive strains (up to 10–20%, depending on the applied tension). The narrow, thin connecting lines accommodate these large strains by delaminating locally from the surface of the elastomer to adopt arc shapes pinned on the ends by the detector pixels (that is, the pixels are not substantially deformed and the interconnect strains are up to ~20–40%), with a mechanics conceptually similar to related responses in stretchable semiconductor ribbons[24]. This process allows the planar-to-spherical geometrical transformation to be accomplished without creating substantial strains in any of the active components of the focal plane array. The hemispherical, elastomeric transfer element, 'inked' with the focal plane array in this manner, enables transfer 'printing' onto a hemispherical glass substrate that has a matching radius of curvature and is coated with a thin layer of a photocurable adhesive. Mounting the resulting system on a printed circuit board with bus lines to external control electronics, establishing electrical connections to pinouts located along the perimeter of the detector array, and integrating with a hemispherical cap fitted with a simple imaging lens completes the hemispherical electronic eye camera. (Details appear in the Supplementary Information.)

The fabrication approach summarized in Fig. 1 can be applied to planar electronics and optoelectronics technologies with nearly arbitrary materials classes and devices, provided that they incorporate appropriately configured compressible interconnects. A key advantage of the strategy is that the most labour-intensive part of the process, that is, formation of the pixel arrays themselves, is fully compatible with the capabilities of existing, planar silicon device manufacturing facilities. Figure 2 outlines the designs and processes implemented in constructing the hemispherical cameras described here. Each pixel in the 16-by-16 imaging array supports two devices—a photodetecting diode and a p–n junction blocking diode—monolithically formed in a single piece of single-crystalline silicon ($500 \times 500\ \mu m^2$ in area, 1.2 μm thick) with a capping layer of polyimide ($560 \times 560\ \mu m^2$ in area, 1–1.5 μm thick): the first device provides local light detection; the second enables current blocking and enhanced isolation for passive matrix readout. Layers of metal above each of the blocking diodes shield them from light, thereby removing their photoresponses. The layout of these layers, the two devices and the electrical connections are illustrated in the schematic view and optical image in Fig. 2a. The pixel-to-pixel interconnects consist of thin layers of patterned metal (360 μm long, 50 μm wide, 3:150:3 nm thick (chromium:gold:chromium)) on thin layers of polyimide (360 μm long, 110 μm wide, 1–1.5 μm thick), spin-cast and patterned in conventional ways.

The images in Fig. 2b, c shows a 16-by-16 array of photodetecting diode–blocking diode pixels transferred onto the surface of a hemispherical, elastomeric transfer element, corresponding to the next-to-last diagram in Fig. 1. The arc-shaped interconnections that enable the planar to hemispherical transformation can be seen clearly. The yields associated with the transfer process and the formation of these types of stretchable connections are high; 100% of the pixels and interconnections in the case of the 16-by-16 arrays have been

reproducibly transferred. Greater than 95% yields have also been demonstrated for the transfer of higher density arrays of passive silicon elements ($20 \times 20\ \mu m^2$ in area, 50 nm thick) and nearest-neighbour connections (20 μm long, 4 μm wide, 50 nm thick) (see Supplementary Fig. 9).

Significant mechanical deformations in the imaging arrays are generated during the transfer process, specifically during the planar to hemispherical transformation of the elastomeric transfer element. Simple mechanics models, based on plate theory and confirmed using established finite element analysis techniques, have been developed to determine the spatial distributions of pixels during the transfer process, as well as the distributions of stresses and

displacements in the interconnections and silicon pixels (see Supplementary Information). These models indicate that the imaging arrays on the hemispherical surface have very small variations (~3% maximum to minimum) in the local pitch and a relatively uniform pitch ~10% smaller than the arrays in the planar, as-fabricated geometry. In addition, the mechanics models predict maximum strains of ~0.01% in the silicon pixels and ~0.3% in the metal of the arc-shaped interconnects for the ~20% change in interconnection length (~10% change in pitch) observed in these systems. Figure 2d is an image of a completed array on a hemispherical glass substrate, corresponding to the last frame in Fig. 1. The high level of engineering control over the fabrication process is evident from the uniformity of the structures that can be transferred to the hemispherical substrate.

Figure 2e shows the current–voltage response of a representative individual pixel in a hemispherical detector array (black, shielded from light; red, exposed to light), addressed by means of row and column electrodes through contact pads at the perimeter of the 16-by-16 array. Similar responses are achieved for individual pixels in planar imaging arrays (see Supplementary Fig. 15). Key features are the strong photoresponse (main frame), the very low reverse bias current (inset), and low crosstalk (inset) between pixels in passive matrix addressing. (Additional details of the device layouts, the electrical properties and the mechanics analysis appear in the Supplementary Information.)

Electrical connections from the row and column contacts at the periphery of the passive matrix array are made to pre-patterned lines on a printed circuit board. The resulting system (Fig. 3a) is interfaced with a computer with specially designed software for acquiring images from the camera. The external electrical connections are formed by evaporating metal over the edge of the concave glass substrate through a flexible shadow mask. Currently, the electrode lines that connect the periphery of the pixel arrays to separate control electronics limit yields and set practical bounds on pixel counts. With unoptimized manual systems, the interconnects from the periphery of the pixel array to the printed circuit board can be registered to an accuracy of ±200 μm. Integration with a hemispherical cap fitted with a simple, single-element lens that provides the imaging optics completes the camera, as illustrated in Fig. 3b, c.

Figure 3d shows images collected with the hemispherical electronic eye camera of Fig. 3a–c. The optical setup for these results used collimated green light (argon ion laser) to illuminate a printed pattern on a transparency film. The transmitted light passed through a simple plano-convex lens (diameter, 25.4 mm; focal length, 35 mm) to form an image on the hemispherical camera (see Supplementary Information and Supplementary Fig. 16). The left-hand frame of Fig. 3d shows the direct output of the camera for the case of an image

Figure 2 | Design and electrical properties of a hemispherical electronic eye camera based on single-crystalline silicon photodetectors and current-blocking p–n junction diodes in a compressible, passive matrix layout.
a, Exploded schematic of the layout of the silicon, metal and polymer associated with a single unit cell in the array. The blocking diode (BD) is in the centre of the cell; the photodetector (PD) is in a serpentine geometry around the BD. **b**, Photograph of a hemispherical PDMS transfer element with a compressible focal plane array on its surface. **c**, Scanning electron microscope image of a portion of the array in **b**, illustrating the compressible interconnects. **d**, Photograph of the array integrated on a hemispherical glass substrate (main frame), optical micrograph of a part of the array (upper right inset) and circuit diagram showing the BDs (black), PDs (red) and electrode crossovers (arcs) in a 2-by-2 section of the system (upper left inset).
e, Electrical properties of a unit cell. The data were measured by contacting the row and column electrodes that address this position in the hemispherical array, by means of pads at the perimeter of the system. The data (black, shielded from light; red, exposed to light) show a high-contrast response to light exposure. Equally importantly, the reverse bias current and leakage from other pixels in the array are both minimal, as shown in the inset.
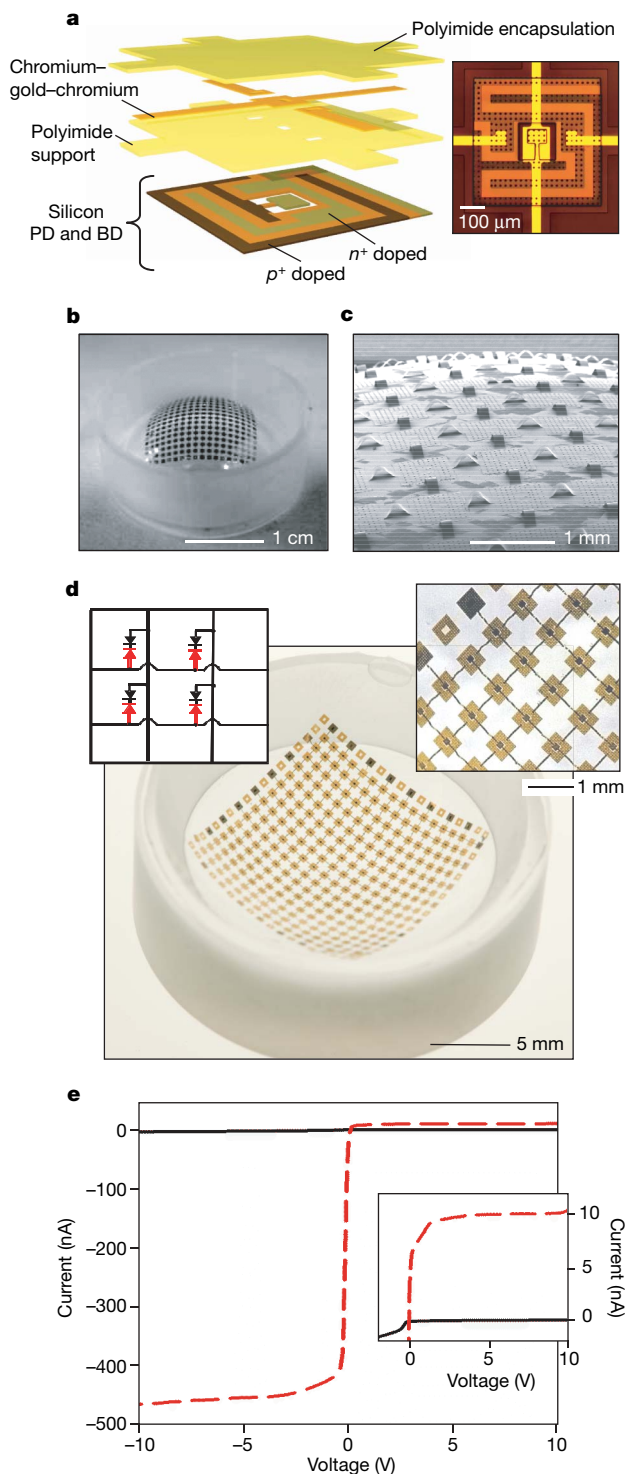
of the top two rows of the standard eye chart[25]. Although the shapes of the letters are clearly resolved, the fine spatial features of the smaller text are not accurately represented, owing to the relatively low numbers of pixels in these cameras. The image quality can be improved by implementing a strategy adapted from biological systems, in which a sequence of images is collected as the camera is eucentrically rotated in the θ and φ directions (θ, azimuthal angle in the plane normal to the optical axis; φ, polar angle measured from the optical axis) relative to the object. Reconstruction, using pixel positions on the hemispherical surface predicted with mechanics models described in the Supplementary Information, yields high-resolution images. The right-hand frame of Fig. 3d is a picture acquired by rapidly scanning a small range of angles (from $-2°$ to $2°$ in both θ and φ) in $0.4°$ increments.
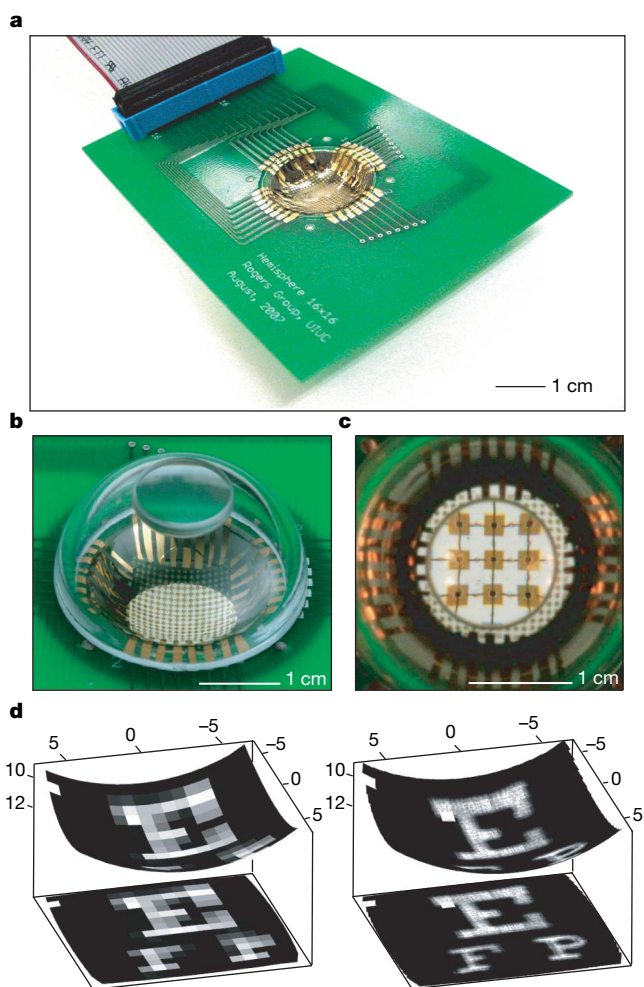

Figure 3 | Photographs of a hemispherical electronic eye camera and representative output images. a, Photograph of a hemispherical focal plane array (centre) mounted on a printed circuit board (green), with external connection to a computer (not shown) through a ribbon cable (upper left). **b**, Photograph of the camera after integration with a transparent (for ease of viewing) hemispherical cap with a simple, single-component imaging lens (top). **c**, Close-up photograph of the system in **b**, as viewed directly through the imaging lens. For the parameters used here, this lens magnifies the focal plane array to show a small, 3-by-3 cluster of pixels. **d**, Greyscale images of the first two rows in an eye chart acquired using a hemispherical camera with a 16-by-16 pixel array, as displayed on a hemispherical surface matching the detector surface (top) and projected onto a plane (bottom). The images on the left and right were acquired without scanning and with scanning (from $-2°$ to $2°$ in the θ and φ directions, in $0.4°$ increments), respectively. The axis scales are in millimetres and are identical in each image.

Even more complex pictures (Fig. 4a, b) can be obtained at high resolution using this simple scanning approach ($-2°$ to $2°$ in both θ and φ, $0.4°$ increments). Inspection of the images suggests that the stitching errors associated with this process are $<40\,\mu m$, thereby validating the accuracy of these models. The nearest-neighbour pixels in the hemispherical camera are separated by $\sim4°$, leading to zero redundancy in generating the tiled picture. These results also demonstrate the high yield of functional pixels, namely $>99\%$ (254 out of 256). Supplementary Figs 18 and 19 show images acquired from each
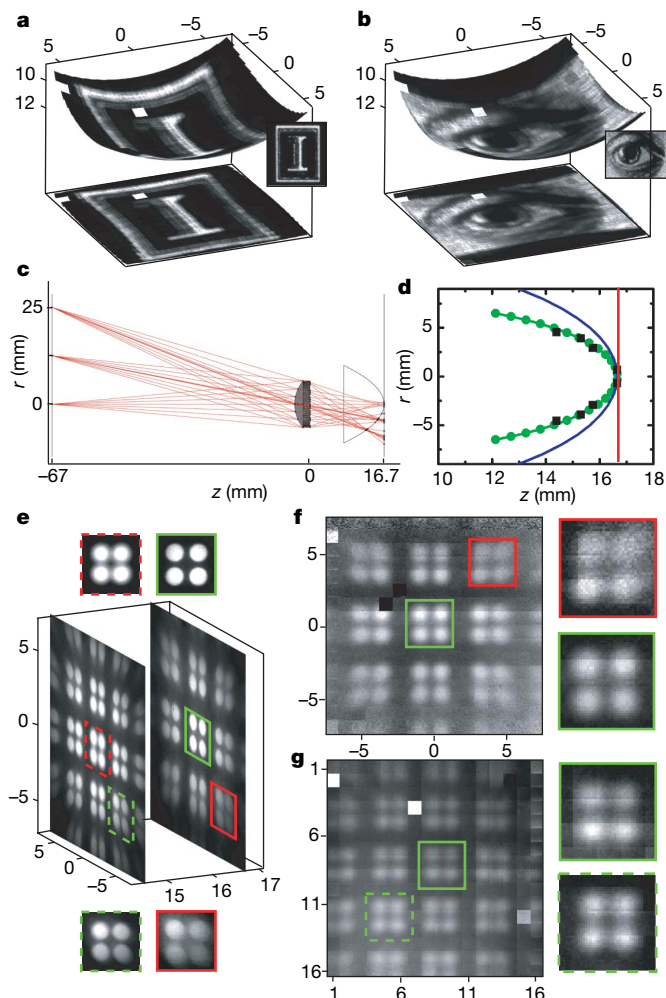

Figure 4 | Enhanced imaging in hemispherical cameras in comparison with planar cameras. High-resolution images of the University of Illinois 'I' logo (**a**) and a drawing of an eye acquired with a hemispherical camera (**b**; insets on the right of **a** and **b** show the original images scanned from the transparency films). **c**, Optics set-up used for imaging and sample ray traces showing a pattern of rays passing through the image and lens onto the detector screens (optimal focal surface and planar camera). Plotted using the Rayica 3.0 package, Optica Software, Champaign, Illinois, USA. **d**, Ray tracing predictions of the curvature of the optimal focal surface (green circles; calculated focal points; green curve, parabolic fit), the detector surface of the hemispherical camera (blue curve), and a planar camera (red curve). **e**, High-resolution photographs of projected images on a planar screen positioned at varying distances from the lens. The left- and right-hand images were acquired at distances $z = 14.40$ mm and $z = 16.65$ mm from the lens, respectively, and demonstrate a shift in optimal focus as a function of detector position. A series of such images was used to estimate the optimal curvilinear focal surface, shown in **d** as black squares. **f, g**, High-resolution images acquired with planar (**f**) and hemispherical (**g**) cameras positioned 16.65 mm from the lens (along the optical axis). All axis scales are in millimetres except for those in **g**, in which pixel number is plotted, and the axes normal to the image planes represent the z direction (optical axis).

pixel when scanned over the entire projected image (from $-40°$ to $40°$ in both θ and φ), further demonstrating the high quality and uniformity of the pixels in the array.

The simple, single-lens system considered here provides a clear example of how curved detectors can improve camera performance. The focusing ability of hemispherical and planar cameras is compared in Fig. 4c–g using fabricated devices, ray tracing software and commercial cameras. An ideal imaging system would perfectly reproduce the image on the detector surface; however, the lens introduces aberrations that degrade the image quality. Complex and expensive optics can reduce the third-order Seidel aberrations for planar detector surfaces, but such aberrations play a significant role in the focusing ability of the simple, single-lens arrangements of interest here[3,26]. A demonstration of focusing abilities requires non-collimated light sources and a wide aperture for a large field of view; thus, the optical test set-up for Fig. 4c–g uses rear-illumination of a pattern printed on paper with halogen lamps and a high-numerical-aperture plano-convex lens (diameter, 12 mm; focal length, 12 mm). Use of optical filters to limit the incident-light wavelength to ~620–700 nm minimizes contributions from chromatic aberrations.

Figure 4c shows the optics arrangement and representative ray traces used to calculate the curvilinear image surface (see Supplementary Information). The calculated surface corresponds, to a good approximation, to a paraboloid of revolution (see Fig. 4d) and is much closer in shape to the hemispherical detector than the planar detector. Figure 4e shows images projected on a planar screen (photographic plastic film) obtained with a commercial camera at two different distances z (left, $z = 14.40$ mm; right, $z = 16.65$ mm) between the screen and lens along the optical axis. The position of best focus shifts from the centre to the edge of the image with decreasing z. The image surface estimated using a series of such photographs is similar to that predicted by the ray tracing theory (see Fig. 4d and Supplementary Figure 20). Figure 4f, g compares images acquired with the fabricated planar and hemispherical cameras, respectively. The hemispherical system has a number of advantages, including more uniform focus from the centre to the edge, a wider field of view, more homogeneous intensity throughout the image and reduced geometric distortions. Many of these features are evident in Fig. 4f, g even at the modest levels of resolution associated with these particular devices.

In conclusion, we note that the compressible optoelectronics and elastomeric transfer element strategies introduced here are compatible with high-resolution focal plane arrays, other more advanced materials systems and device designs, and refined substrate shapes (for example parabolic or other aspherical surfaces). Demonstrating these possibilities, exploring applications in other areas, and defining the fundamental limits associated with the materials, layouts and mechanics of the compressible interconnects represent promising topics for future work.

METHODS SUMMARY

Fabrication of hemispherical cameras. A hemispherical, elastomeric transfer element was molded in poly(dimethylsiloxane) (Sylgard 184, Dow Corning) by curing a liquid prepolymer between convex and concave lenses with identical radii of curvature (12.9 mm, CVI Laser Optics). Coordinated radial stretching of the transfer element such that the hemispherical surface could be reversibly deformed to a planar drumhead surface was performed using a custom-designed mechanical stage. A passive matrix focal plane array was fabricated separately on a planar silicon-on-insulator wafer (1.2-μm-thick silicon layer on a 400-nm-thick silicon dioxide insulator layer, Soitec) using conventional semiconductor processing. The buried oxide layer in the silicon-on-insulator wafer was removed after complete fabrication of the detector array by etching with concentrated hydrofluoric acid and this wafer was contacted to the radially tensioned transfer element in its planar drumhead shape. The focal plane array was lifted onto this planar elastomeric transfer element after peeling away the wafer and remained adhered through intermolecular van der Waals interactions. Relaxing the tension on the planar elastomeric transfer element transformed the focal plane array and transfer element into approximately the original hemispherical surface. The focal plane array was then transfer printed from the hemispherical transfer

element onto a matching concave glass substrate coated with a thin layer of photocurable adhesive (NOA 73, Norland). The hemispherical substrate was mounted in a printed computer board and electrical connections to external pinouts were made from metal evaporated through an elastomeric shadow mask.
Imaging with hemispherical cameras. The hemispherical cameras collected images using two distinct set-ups. Collimated laser light (argon ion laser; Figs 3d and 4a, b) and non-collimated light sources (halogen lamps; Figs 4e–g) illuminated a pattern printed on transparency and paper screens, respectively. The transmitted light then passed through a single plano-convex lens to form an image on the hemispherical camera.

1. Land, M. F. & Nilsson, D.-E. *Animal Eyes* (Oxford Univ. Press, New York, 2002).
2. Goldsmith, T. H. Optimization, constraint, and history in the evolution of eyes. *Q. Rev. Biol.* **65**, 281–322 (1990).
3. Walther, A. *The Ray and Wave Theory of Lenses* (Cambridge Univ. Press, Cambridge, UK, 1995).
4. Swain, P. & Mark, D. Curved CCD detector devices and arrays for multi-spectral astrophysical applications and terrestrial stereo panoramic cameras. *Proc. SPIE* **5499**, 281–301 (2004).
5. Grayson, T. Curved focal plane wide field of view telescope design. *Proc. SPIE* **4849**, 269–274 (2002).
6. Khang, D. Y., Jiang, H., Huang, Y. & Rogers, J. A. A stretchable form of single crystal silicon for high performance electronics on rubber substrates. *Science* **311**, 208–212 (2006).
7. Jackman, R. J., Wilbur, J. L. & Whitesides, G. M. Fabrication of submicrometer features on curved substrates by microcontact printing. *Science* **269**, 664–666 (1995).
8. Paul, K. E., Prentiss, M. & Whitesides, G. M. Patterning spherical surfaces at the two-hundred nanometer scale using soft lithography. *Adv. Funct. Mater.* **13**, 259–263 (2003).
9. Miller, S. M., Troian, S. M. & Wagner, S. Direct printing of polymer microstructures on flat and spherical surfaces using a letterpress technique. *J. Vac. Sci. Technol. B* **20**, 2320–2327 (2002).
10. Childs, W. R. & Nuzzo, R. G. Patterning of thin-film microstructures on non-planar substrate surfaces using decal transfer lithography. *Adv. Mater.* **16**, 1323–1327 (2004).
11. Lee, K. J., Fosser, K. A. & Nuzzo, R. G. Fabrication of stable metallic patterns embedded in poly(dimethylsiloxane) and model applications in non-planar electronic and lab-on-a-chip device patterning. *Adv. Funct. Mater.* **15**, 557–566 (2005).
12. Lima, O., Tan, L., Goel, A. & Negahban, M. Creating micro- and nanostructures on tubular and spherical surfaces. *J. Vac. Sci. Technol. B* **25**, 2412–2418 (2007).
13. Radtke, D. & Zeitner, U. D. Laser-lithography on non-planar surfaces. *Opt. Express* **15**, 1167–1174 (2007).
14. Ruchehoeft, P. & Wolfe, J. C. Optimal strategy for controlling linewidth on spherical focal surface arrays. *J. Vac. Sci. Technol. B* **18**, 3185–3189 (2000).
15. Xia, Y. *et al.* Complex optical surfaces formed by replica molding against elastomeric masters. *Science* **273**, 347–349 (1996).
16. Hsu, P. I. *et al.* Spherical deformation of compliant substrates with semiconductor device islands. *J. Appl. Phys.* **95**, 705–712 (2004).
17. Hsu, P. I. *et al.* Effects of mechanical strain on TFTs on spherical domes. *IEEE Trans. Electron. Dev.* **51**, 371–377 (2004).
18. Jacobs, H. O., Tao, A. R., Schwartz, A., Gracias, D. H. & Whitesides, G. M. Fabrication of a cylindrical display by patterned assembly. *Science* **296**, 323–325 (2002).
19. Zheng, W., Buhlmann, P. & Jacobs, H. O. Sequential shape-and-solder-directed self-assembly of functional microsystems. *Proc. Natl Acad. Sci. USA* **101**, 12814–12817 (2004).
20. Boncheva, M. *et al.* Magnetic self-assembly of three-dimensional surfaces from planar sheets. *Proc. Natl Acad. Sci. USA* **102**, 3924–3929 (2005).
21. Boncheva, M. & Whitesides, G. M. Templated self-assembly: Formation of folded structures by relaxation of pre-stressed, planar tapes. The path to ubiquitous and low-cost organic electronic appliances on plastic. *Adv. Mater.* **17**, 553–557 (2005).
22. Huang, Y. Y. *et al.* Stamp collapse in soft lithography. *Langmuir* **21**, 8058–8068 (2005).
23. Zhou, W. *et al.* Mechanism for stamp collapse in soft lithography. *Appl. Phys. Lett.* **87**, 251925 (2005).
24. Sun, Y. *et al.* Controlled buckling of semiconductor nanoribbons for stretchable electronics. *Nature Nanotechnol.* **1**, 201–207 (2006).
25. Begbie, G. H. *Seeing and the Eye* 92–93 (Natural History Press, Garden City, New York, 1969).
26. Born, M. & Wolf, E. *Principles of Optics* 7th edn (Cambridge Univ. Press, New York, 1999).

Author Contributions H.C.K., M.P.S., V.M. and J.A.R. designed the experiments. H.C.K., M.P.S., J.S., V.M., W.M.C, C.-J.Y., J.B.G., J.X., S.W., Y.H. and J.A.R. performed the experiments and analysis. H.C.K., M.P.S., J.S., Y.H. and J.A.R. wrote the paper.

Author Information Reprints and permissions information is available at www.nature.com/reprints. Correspondence and requests for materials should be addressed to J.A.R. (jrogers@uiuc.edu) and Y.H. (y-huang@northwestern.edu).